A Modified Acellular Amniotic Membrane Hydrogel Promotes Wound Healing by Regulating Macrophage Polarization

Tao Wang [†], Zhiyuan Zhu [†], Wei Hua, Siliang Xue [*]

Posted Date: 2 September 2025

doi: 10.20944/preprints202509.0226.v1

Keywords: human acellular amniotic membrane; hydrogel; THP-1 cells; wound healing; immunomodulation

 doi:10.20944/preprints202509.0226.v1

Article

A Modified Acellular Amniotic Membrane Hydrogel Promotes Wound Healing by Regulating Macrophage Polarization

Tao Wang †, Zhi-Yuan Zhu †, Wei Hua and Si-Liang Xue *

Department of Dermatology, West China Hospital, Sichuan University, Chengdu, China

* Correspondence: author: Si-Liang Xue, M.D. Email address: xuesiliang@wchscu.cn

† These authors contributed equally to this work.

Abstract

Amniotic membrane has been widely utilized and studied as a tissue-engineered material for decellularized bioscaffolds to promote skin wound healing. However, human acellular amniotic membrane (HAAM) has limitations, such as poor mechanical properties, rapid degradation, and challenges in handling and use. In this study, VEGF-loaded GG-HA hydrogels were combined with DAPT-loaded decellularized biological amniotic membrane to develop novel amniotic membrane-derived materials (VEGF-GG-HA & DAPT-HAAM). Furthermore, in vitro experiments were conducted using THP-1 cells (Tohoku Hospital Pediatrics-1 cell line) to assess the immunomodulatory effects of these amniotic membrane-derived materials on macrophages and inflammatory factors. The experimental groups included DAPT-HAAM, VEGF-GG-HA, and VEGF-GG-HA & DAPT-HAAM. Following THP-1 cell culture, the biocompatibility of the new grafts, along with the levels of cytokines and matrix metalloproteinases, were evaluated using CCK-8 assays, enzyme-linked immunosorbent assays (ELISA), quantitative real-time PCR, Western blot analysis, and immunohistochemical staining. The results demonstrated that the novel grafts (VEGF-GG-HA & DAPT-HAAM) exhibited good biocompatibility and promoted the secretion of IL-10, TNF-α, TGF-β, MMP1, and MMP3, while suppressing excessive TGF-β overexpression. Overall, these new grafts showed enhanced performance in promoting monocyte proliferation, regulating cytokine secretion, and modulating protein expression. Additionally, they induced the transition from M1-type macrophages to anti-inflammatory M2-type macrophages, facilitated vascular remodeling of peri-wound tissues, improved the inflammatory environment, reduced fibrous proliferation, and prevented scar formation, ultimately accelerating wound healing.

Keywords: human acellular amniotic membrane; hydrogel; THP-1 cells; wound healing; immunomodulation

1. Introduction

Recent advances in skin tissue engineering and wound healing primarily focus on developing partial or complete skin substitutes, with the ultimate goal of restoring the normal structure of the skin. Amniotic membrane has been extensively studied and utilized as a tissue-engineered material for decellularized bioscaffolds to promote skin wound healing, owing to its antimicrobial, hemostatic, anti-inflammatory, adhesion-preventing, antifibrotic, and immunosuppressive properties[1]. Our team has utilized human acellular amniotic membrane (HAAM) for treating defects in the lower third of the nasal skin and external ear skin, demonstrating significant benefits in accelerating wound hemostasis, reducing infection, and promoting wound repair[2,3]. However, HAAM also has limitations, including poor mechanical properties, rapid degradation, challenges in implantation, and suboptimal outcomes for large or total skin defects. Therefore, it is essential to modify the amniotic membrane in a practical and achievable manner to address these shortcomings.

 doi:10.20944/preprints202509.0226.v1

Angiogenesis is a crucial step in wound healing, and abnormal vascularization can lead to delayed healing or poor-quality tissue regeneration, resulting in impaired wound recovery. Biomaterials, cells, and cytokines can enhance the quality of wound vascularization and promote more effective wound healing[4]. Among these, vascular endothelial growth factor (VEGF), an inflammatory mediator released by macrophages during the early stages of inflammation, promotes fibroblast migration, activates microvascular endothelial cells (ECs), and facilitates the formation of neovascularized blood vessels and an abundant extracellular matrix[5]. Additionally, it has been demonstrated that the GG-HA sponge-like hydrogel, created by combining hyaluronic acid (HA) with gelation agent (GG), exhibits a semi-interpenetrating network structure and can continuously release HA oligomers, significantly enhancing tissue vascularization and promoting wound healing[6]. Thus, the combination of vascular endothelial growth factor (VEGF) and the GG-HA sponge-like hydrogel synergistically enhances wound vascularization and accelerates wound healing.

During wound healing, Notch signaling promotes the differentiation of epidermal and follicular stem cells, accompanied by keratinocyte synthesis, fibroblast proliferation and migration, angiogenesis, and extracellular matrix deposition[4]. Studies have shown that inhibition of the Notch-1 signaling pathway by the γ-secretase inhibitorN-[N-(3,5-difluorophenacetyl)-L-alanylhydrazide]-S-phenylglycine t-butyl ester (DAPT) reduced experimentally induced dermal and cutaneous fibrosis in systemic sclerosis, demonstrating the preventive and therapeutic effects of low-dose Notch inhibitor treatment on dermatofibrosis[7].

Additionally, when implants are used to promote wound healing, macrophages—the key cells of the early inflammatory response—release a variety of pro- and anti-inflammatory cytokines, playing a crucial role in the post-implantation inflammatory response and ultimately determining the wound healing outcome. Therefore, the use of modified polymers to modulate macrophage-driven immune responses and improve wound healing outcomes is an active area of current research[8]. Numerous studies have shown that inhibition of the Notch-1 signaling pathway promotes the shift in macrophage recruitment from M1-type to M2-type dominance, along with the release of anti-inflammatory factors such as IL-10, thereby attenuating inflammation and reducing tissue damage and fibrosis[9-12]. Therefore, in this study, Notch-1 signaling pathway inhibitors were integrated into a novel amniotic membrane-derived material to promote macrophage immunomodulation and reduce fibroplasia, thereby enhancing wound healing.

In summary, this study involved wrapping VEGF-loaded GG-HA hydrogels around DAPT-loaded decellularized biological amniotic membrane to create new amniotic membrane-derived materials (VEGF-GG-HA & DAPT-HAAM). In addition, in vitro experiments using the THP-1 cell line were conducted to evaluate the effects of these materials on macrophage immunomodulation and inflammatory factors.

2. Materials and Methods

2.1. Materials Preparation

2.1.1. Preparation of DAPT-HAAM

Our previously published papers provide detailed information on the source and production process of HAAM[3]. DAPT microspheres were prepared as follows: Gelatin and agar were dissolved in deionized water by heating and stirring, after which DAPT lyophilized powder was added and mixed thoroughly. The mixture was then homogenized with a limonene receiving solution using a syringe pump, followed by the addition of HAAM for precipitation. The precipitate was washed with methanol to obtain DAPT-HAAM. The mixture was freeze-dried using a lyophilization agent for 24 hours and sterilized with ethylene oxide. The morphology, structural porosity, and pore size were observed using scanning electron microscopy.

 doi:10.20944/preprints202509.0226.v1

2.1.2. Preparation of VEGF-GG-HA

HA was dissolved in deionized water, and Gelzan gel powder was added and stirred at 90°C for 30 minutes. The mixture was then combined with minimum essential medium (MEM-α) to form a hydrogel, which was stabilized in phosphate-buffered saline for 28 hours. The hydrogel was frozen at -80°C and freeze-dried for 3 days to obtain the dried polymerized network structure of GG-HA, which was subsequently rehydrated to form the sponge-like hydrogel GG-HA. VEGF microspheres were prepared using the same method as DAPT microspheres, then added to the dissolved hydrogel GG-HA. An ultrasonic device was used to promote the uniform distribution of VEGF microspheres within the hydrogel, resulting in the formation of VEGF-GG-HA. The morphology, structural porosity, and pore size of the material were observed using scanning electron microscopy.

2.1.3. Preparation of VEGF - GG - HA&DAPT - HAAM

VEGF-GG-HA was prepared as a circular film with a thickness of 0.1 cm and a diameter of 1 cm on a mold. A piece of DAPT-HAAM, with a diameter of 0.8 cm, was placed between two layers of VEGF-GG-HA hydrogel. The assembly was heated to the sol-gel transition temperature and then cooled to induce cross-linking of the upper and lower gels, resulting in the formation of DAPT-HAAM & VEGF-GG-HA.

2.2. In Vitro Studies

2.2.1. Assessment of Cell Activity by the CCK-8 Assay

DAPT-HAAM, VEGF-GG-HA, and VEGF-GG-HA&DAPT-HAAM were added to each well as experimental groups (n = 6), while blank groups were included as control. In each well of a 96-well plate, 100 μL of 10% fetal bovine serum and RPMI-1640 medium was added. Then, 100 μL of cell suspension containing 5000 THP-1 cells was seeded into each well. The plate was incubated in a constant-temperature cell culture incubator at 37°C with 5% CO2. CCK-8 assays were performed on days 1, 2, 3, and 4. Specifically, the initial cell culture medium was aspirated and replaced with fresh medium, followed by the addition of 10 μL of CCK-8 solution to each well. After a 3-hour incubation period, the absorbance at 450 nm was measured using a spectrophotometer.

2.2.2. Determination of Cytokine Profile by ELISA and Quantitative Real-Time PCR

THP-1 cells were seeded into a 96-well plate containing culture medium, followed by the addition of DAPT-HAAM, VEGF-GG-HA, VEGF-GG-HA&DAPT-HAAM, and blank hydrogel at various concentrations. The plate was incubated in a constant-temperature cell culture incubator at 37°C with 5% CO2. After 48 hours of cell culture, the cell supernatant was aspirated and centrifuged (1000 rpm, 5 min). The supernatant was then used for cytokine measurement via indirect ELISA, following the manufacturer's instructions (BioMedBAY Co., Ltd.), including IL-10 (70-EK210/4-48) and tumor necrosis factor-α (TNF-α) (70-EK282HS-48). Additionally, after 24 hours of cell culture, as described above, the cells were lysed, and total RNA was extracted using Trizol lysate (Invitrogen, 15596018CN). RNA concentration and quality were measured using a DU800 UV/Vis spectrophotometer (Beckman Coulter, United States). According to the manufacturer's instructions, mRNA was reverse transcribed using a cDNA Synthesis Kit (Roche, 05091284001). The expression of IL-10 and TNF-α genes was detected by qPCR after reverse transcription and cDNA synthesis. The primer sequences for the two cytokines are as follows:

- IL-10: Forward Primer: TCAAGGCGCATGTGAACTCC (Length: 20, Tm: 62.8°C), Reverse Primer: GATGTCAAACTCACTCATGGCT (Length: 22, Tm: 60.3°C).
- TNF-α: Forward Primer: CCTCTCTCTCTAATCAGCCCTCTG (Length: 22, Tm: 60.8°C), Reverse Primer: GAGGACCTGGGGAGTAGATGAG (Length: 21, Tm: 60.2°C).

 doi:10.20944/preprints202509.0226.v1

2.2.3. Western Blotting Analysis

After 24 hours of stimulation, cells were lysed in RIPA buffer to quantify total cell proteins. Protein concentrations in the cell lysate supernatants were determined using a bicinchoninic acid (BCA) protein assay kit (Thermo Scientific, Rockford, United States). Extracted proteins were then separated on 10% SDS-PAGE gels and transferred to polyvinylidene difluoride (PVDF) membranes (Millipore Immobilon, United States). After blocking with 3% BSA (Biosharp, CN, United States) for 2 hours at room temperature, the membranes were incubated with primary antibodies and horseradish peroxidase (HRP)-conjugated secondary antibodies. MMP1, MMP3, and TGF-β expression were measured using western blotting (WB). β-Actin protein served as the internal reference. Chemiluminescence bands were quantified using an enhanced chemiluminescence (ECL) detection kit (Pierce, 35055) and the ChemiDocTM XRS Imaging system (Bio-Rad, United States), with analysis performed using ImageJ.

2.2.4. Immunohistochemical Staining

DAPT-HAAM, VEGF-GG-HA, VEGF-GG-HA&DAPT-HAAM, and blank hydrogel were aseptically placed into a 96-well plate, followed by the addition of THP-1 cell suspension to each well. One milliliter of culture medium was added to each well. Calcein-AM and ethidium homodimer-1 (Live/Dead Cell Viability, Invitrogen, USA) were prepared 30 minutes in advance and allowed to reach room temperature. The staining working solution was prepared according to the manufacturer's instructions. On the third day of culture, the initial culture medium was removed, and the wells were gently washed three times with PBS. Two hundred microliters of staining working solution were added to each well to cover the bottom of the plate. The plate was incubated at room temperature in the dark for 30 minutes. After incubation, the wells were washed gently with PBS three times, with each wash lasting 3 minutes. Green and red fluorescence images were captured at the same positions using a fluorescence microscope and recorded.

2.3. Statistical Analysis

Data were analyzed using GraphPad Prism 8.0 software (GraphPad Software Inc., San Diego, CA, USA) and are presented as mean ± standard deviation (X ± SD). Normality tests were performed on each dataset, with normally distributed data analyzed using the Chi-square test. Abnormally distributed data were analyzed using one-way analysis of variance (one-way ANOVA). Differences were considered statistically significant at $P < 0.05$.

3. Results

3.1. Characterization of VEGF - GG - HA and DAPT - HAAM

We examined the microstructure of VEGF-GG-HA and DAPT-HAAM using scanning electron microscopy (SEM). The SEM images revealed that both samples exhibited a dense pore structure. DAPT microspheres were spherical in shape, with a particle size of approximately 100 nm, and were successfully enriched on decellularized amniotic membranes (Fig. 1A). VEGF microspheres, also spherical in shape, had a particle size of approximately 130 nm (Fig. 1B).

 doi:10.20944/preprints202509.0226.v1

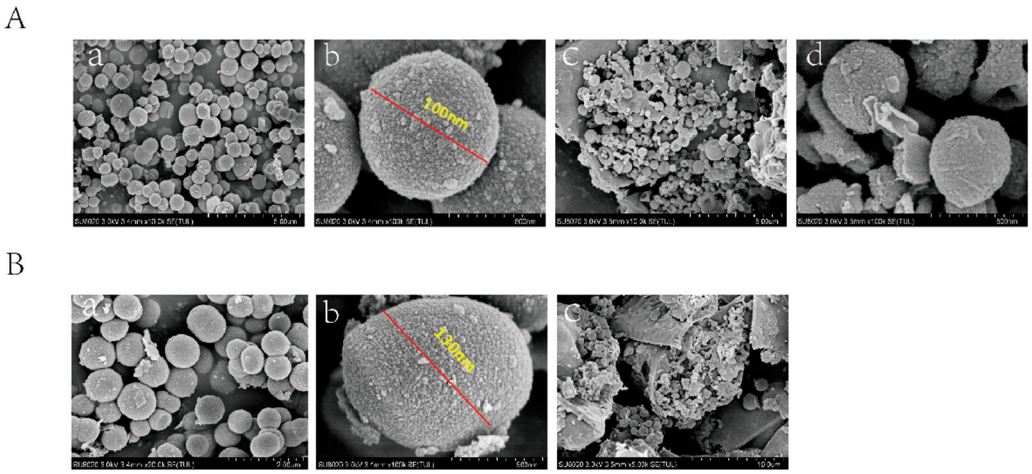

Figure 1. SEM image and aperture frequency distribution. SEM images of DAPT - HAAM, VEGF - GG - HA are shown in panels A, B, respectively.

3.2. In vitro Cell Experiment

3.2.1. Assessment of Cell Activity by the CCK-8 Assay

The results of the CCK-8 assay demonstrated that, compared to the blank control group, cell viability in all three experimental groups began to increase after 24 hours of cell culture, with a significant increase in viability observed at 72 and 96 hours ($p < 0.001$, Fig. 2). The DAPT & VEGF microsphere group exhibited the highest cell viability at all time points, followed by the VEGF microsphere group and the DAPT microsphere group. Furthermore, significant differences in cell viability were observed between the DAPT & VEGF microsphere group and both the VEGF microsphere group and the DAPT microsphere group ($p < 0.001$, Fig. 2). These results indicated that all three biomaterials significantly promoted the proliferation of THP-1 cells, with the VEGF-GG-HA & DAPT-HAAM biomaterials demonstrating superior ability to enhance cell proliferation compared to the VEGF or DAPT biomaterials alone. The CCK-8 assay results also suggested that the VEGF-GG-HA & DAPT-HAAM biomaterials exhibited good biocompatibility.

 doi:10.20944/preprints202509.0226.v1

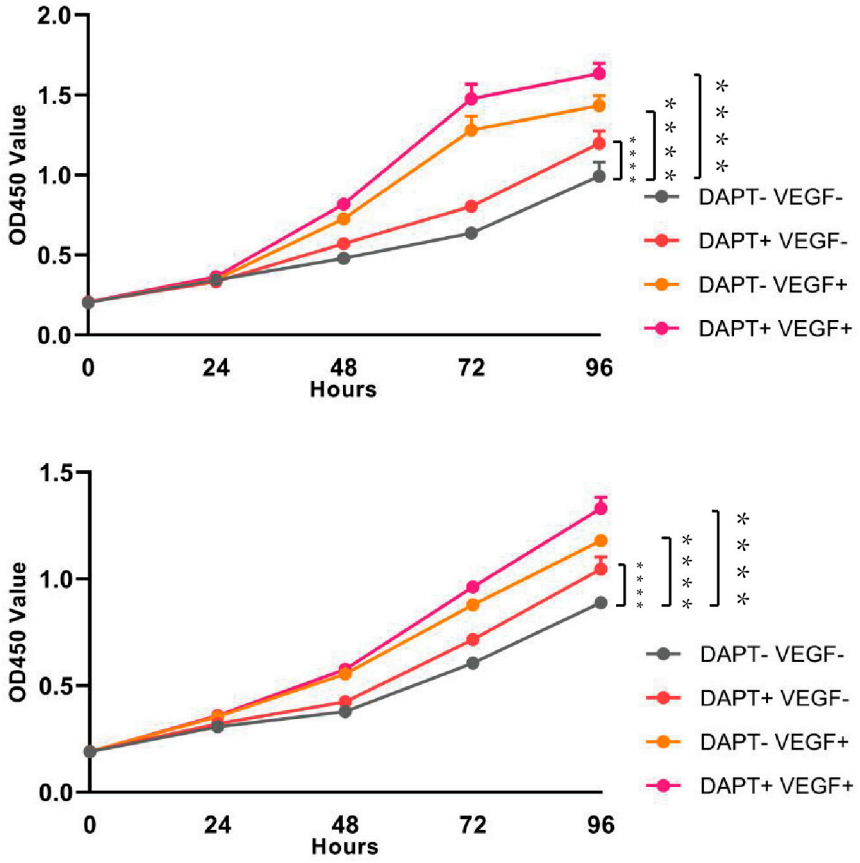

Figure 2. Assessment of cell activity by the CCK-8 assay, DAPT-VEGF-, DAPT+VEGF-, DAPT-VEGF+, DAPT+VEGF+ represent control, DAPT-HAAM, VEGF-GG-HA, VEGF-GG-HA&DAPT-HAAM, respectively.

3.2.2. Determination of Cytokine Profile by ELISA

The ELISA results demonstrated that IL-10 levels were significantly higher in all three experimental groups compared to the blank control group ($p < 0.0001$, Fig. 3A). The DAPT & VEGF microsphere group exhibited the greatest increase, followed by the VEGF microsphere group and the DAPT microsphere group. Additionally, significant differences in IL-10 levels were observed between the DAPT & VEGF microsphere group, VEGF microsphere group, and DAPT microsphere group ($p < 0.0001$, Fig. 3A). These results indicated that all three biomaterials promoted the conversion of macrophage recruitment from M1-type to M2-type and enhanced IL-10 secretion, with the VEGF-GG-HA & DAPT-HAAM biomaterials demonstrating the strongest ability.

 doi:10.20944/preprints202509.0226.v1

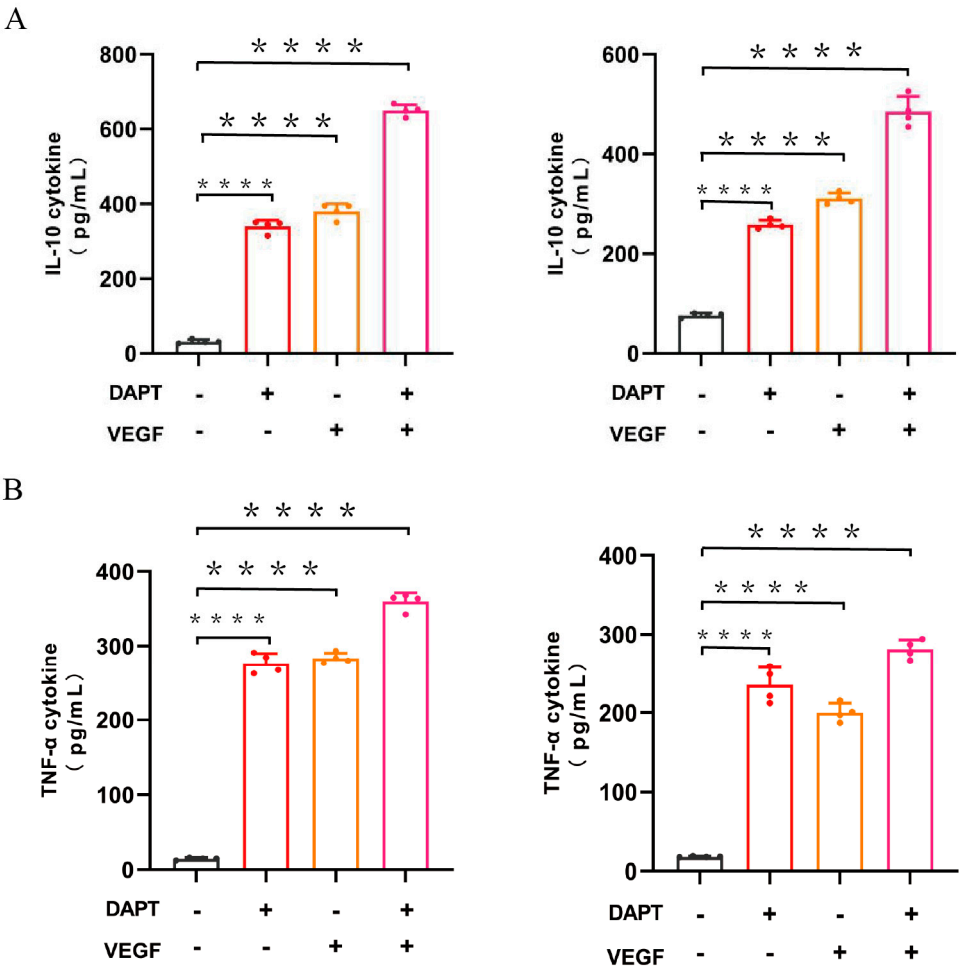

Figure 3. Quantification of the levels of cytokines, such as IL-10, TNF-α were analyzed by ELISA. Data represent the mean ± SD. ****, P < 0.0001.

The ELISA results also showed that TNF-α levels were significantly increased in all three experimental groups compared to the blank control group ($p < 0.0001$, Fig. 3B), with the greatest increase observed in the DAPT & VEGF microsphere group. Moreover, significant differences in TNF-α levels were found between the DAPT & VEGF microsphere group and both the VEGF microsphere group and the DAPT microsphere group ($p < 0.0001$, Fig. 3B). These results indicated that all three biomaterials promoted TNF-α secretion from M1-type macrophages, with the VEGF-GG-HA & DAPT-HAAM biomaterials exhibiting the strongest effect.

3.2.3. Determination of Cytokine Profile by QPCR

The qPCR results demonstrated that the IL-10 mRNA expression level was significantly higher in all three experimental groups compared to the blank control group ($p < 0.0001$, Fig. 4A), with the greatest increase observed in the DAPT & VEGF microsphere group. These results indicated that all three biomaterials promoted the conversion of macrophage recruitment from M1-type to M2-type and enhanced IL-10 secretion, with VEGF-GG-HA & DAPT-HAAM biomaterials exhibiting the strongest effect. Additionally, the expression level of TNF-α was significantly higher in the DAPT & VEGF microsphere group compared to the blank control group ($p < 0.0001$, Fig. 4B). This finding suggested that the DAPT & VEGF microsphere group effectively promoted the secretion of TNF-α from M1-type macrophages. Biomaterials containing only VEGF or DAPT had a weaker ability to promote TNF-α secretion.

 doi:10.20944/preprints202509.0226.v1

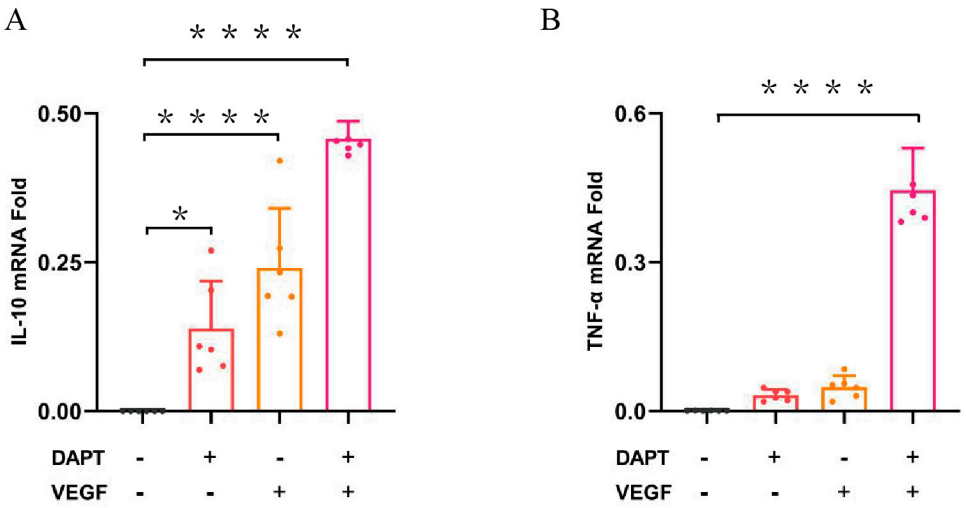

Figure 4. Quantification of the levels of cytokines, such as IL-10, TNF-α were analyzed by ELISA. Data represent the mean ± SD. *, P < 0.01, ****, P < 0.0001.

3.2.4. Western Blotting Analysis

The results showed that, compared with the blank control group, the expression level of MMP1 protein in the DAPT & VEGF microsphere group significantly increased after 48 and 96 hours of cell culture, with the highest expression observed among the three experimental groups ($p < 0.001$, Fig. 5A). However, there was no significant increase in MMP1 protein expression after 72 hours of cell culture ($p > 0.05$, Fig. 5A). In the DAPT microsphere group, MMP1 protein expression was significantly elevated after 48 and 72 hours of cell culture, with the highest expression at 72 hours ($p < 0.001$, Fig. 5A). After 96 hours, the MMP1 protein expression level was lower than that of the control group ($p < 0.01$, Fig. 5A). For the VEGF microsphere group, MMP1 protein expression was slightly elevated after 72 and 96 hours of culture ($p < 0.001$, Fig. 5A). These results indicate that the DAPT & VEGF microsphere group could significantly promote MMP1 protein secretion after 48 and 96 hours, but the effect was insufficient at 72 hours. The DAPT microsphere group significantly promoted MMP1 protein secretion after 48 and 72 hours, with the strongest effect at 72 hours. In contrast, VEGF microsphere group did not show significant promotion of MMP1 secretion.

 doi:10.20944/preprints202509.0226.v1

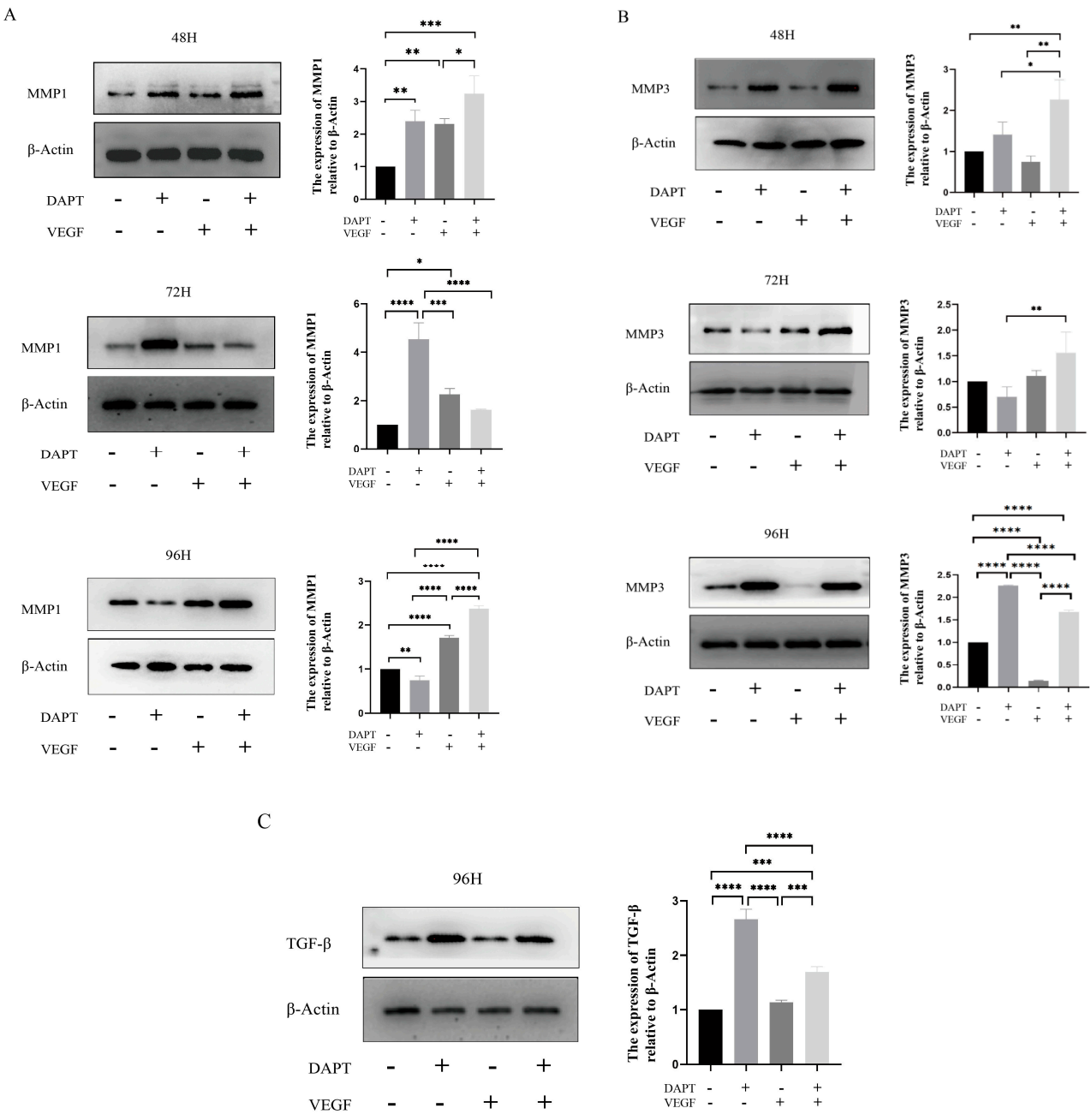

Figure 5. Expression of the levels of TGF-β, MMP1, MMP3 were analyzed by Western Blotting Analysis. Data represent the mean ± SD. *, P < 0.05, **, P < 0.01, ***, P < 0.001, ****, P < 0.0001.

For MMP3 protein, the expression level was significantly increased in the DAPT & VEGF microsphere group after 48, 72, and 96 hours of cell culture, with the highest expression observed after 48 and 72 hours ($p < 0.01$, Fig. 5B). In the DAPT microsphere group, MMP3 protein expression significantly increased after 48 and 96 hours, with the highest expression at 96 hours ($p < 0.0001$, Fig. 5B). However, after 72 hours, MMP3 expression was lower than that of the control group. The VEGF microsphere group did not show significant increases in MMP3 expression at any time point ($p > 0.05$, Fig. 5B). These results suggest that the DAPT & VEGF microsphere group significantly promoted MMP3 protein secretion after 48, 72, and 96 hours, with the strongest effect at 48 and 72 hours. The DAPT microsphere group significantly promoted MMP3 protein secretion after 48 and 96 hours, with the strongest effect at 96 hours. VEGF microsphere group did not significantly promote MMP3 secretion.

 doi:10.20944/preprints202509.0226.v1

For TGF-β protein, the expression level in both the DAPT & VEGF microsphere group and the DAPT microsphere group significantly increased after 96 hours of cell culture, with the highest expression observed in the DAPT microsphere group ($p < 0.001$, Fig. 5C). No significant increase in TGF-β expression was observed in the VEGF microsphere group ($p > 0.05$, Fig. 5C). These results indicate that the DAPT & VEGF microsphere group and the DAPT microsphere group could significantly promote TGF-β secretion after 96 hours of cell culture, with the DAPT microsphere group showing a stronger effect. However, the VEGF microsphere group did not significantly promote TGF-β secretion. The findings suggest that while the DAPT & VEGF microsphere group can promote TGF-β secretion, it also limits the over-secretion of TGF-β.

3.2.5. Immunohistochemical Staining

The results showed that the DAPT & VEGF microsphere group could promote MMP1 protein secretion after 72 hours of cell culture.

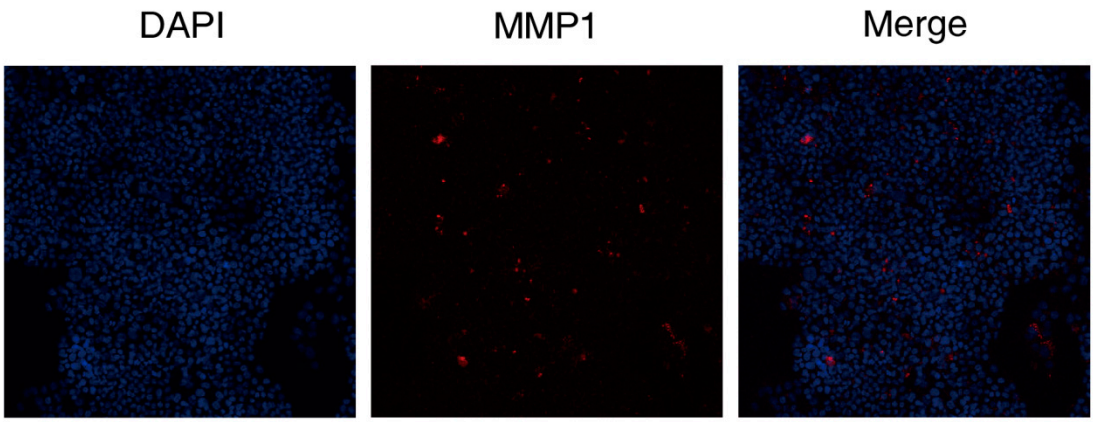

Figure 6. Expression of the levels of MMP were analyzed by immunohistochemical staining. Representative immunocytochemistry images of the expression of MMP1 (red) by DAPT&VEGF. Nuclei were stained with DAPI (blue).

4. Discussion

To overcome the limitations of decellularized bio-amniotic membrane and maximize its ability to promote wound healing, this study explored the modification of decellularized biological amniotic membrane using VEGF, GG-HA sponge-like hydrogel, and DAPT. The new graft demonstrated superior performance in promoting monocyte proliferation, regulating cytokine secretion, and influencing protein expression.

Pro-inflammatory M1-type macrophages dominate the early phase of wound healing, with up to 85% of macrophages exhibiting the M1 phenotype[13], these macrophages produce a strong pro-inflammatory response and play a crucial role in host defense and necrotic tissue clearance[14]. One of the key cytokines, TNF-α, accelerates immune cell infiltration into the wound during the pre-healing phase, creating an inflammatory microenvironment that facilitates the initiation and promotion of neovascularization. TNF-α indirectly induces the secretion of VEGF by promoting inflammatory responses, which in turn stimulates the differentiation of endothelial progenitor cells into functional endothelial cells, aids in VEGF-mediated capillary regeneration, and enhances granulation tissue formation, ultimately improving the wound healing process[15-18]. VEGF is a heparin-binding growth factor specific to vascular endothelial cells, which not only induces the differentiation of embryonic stem cells into endothelial progenitor cells and endothelial cells in vitro but also acts as a key regulator of wound vascularization. It promotes endothelial cell migration and neovascularization,

 doi:10.20944/preprints202509.0226.v1

playing a pivotal role in the formation of new blood vessels at the wound site[19,20]. It is evident that TNF-α and VEGF exert synergistic effects in angiogenesis, vascular permeability, and the regeneration of traumatized tissue. The new grafts developed in this study enhance TNF-α secretion while providing the VEGF necessary for wound healing. The combined action of these factors promotes vascular remodeling in the periwound tissues, improves the inflammatory environment, and accelerates the wound healing process.

The transition from M1-type to M2-type macrophages signifies the shift from the inflammatory phase to the repair phase of wound healing[21]. IL-10 and TGF-β can induce the transition of M1-type macrophages to the anti-inflammatory M2-type macrophages. At the same time, M2-type macrophages secrete anti-inflammatory factors such as IL-10 to counteract inflammatory responses, while also releasing repair-promoting cytokines like VEGF and TGF-β to stimulate angiogenesis and collagen deposition, thereby accelerating wound healing[22]. The new material can promote the secretion of IL-10 and TGF-β, facilitating the transition from M1-type to M2-type macrophages, which is beneficial for wound healing. This effect may be attributed to the inclusion of a Notch-1 signaling pathway inhibitor in the new material, which enhances the shift in macrophage recruitment from M1-type to M2-type and encourages the release of anti-inflammatory factors. Additionally, studies have shown that local increases in TGF-β are associated with elevated levels of vascular endothelial growth factor (VEGF)[23]. Thus, VEGF in the new grafts plays a crucial role in promoting TGF-β secretion. TGF-β is involved in several processes during wound healing, including inflammation, stimulating angiogenesis, fibroblast proliferation, collagen synthesis and deposition, as well as the remodeling of the extracellular matrix[24,25]. However, research indicates that elevated levels of TGF-β are associated with the deposition of extracellular matrix (ECM) in the wound, promoting the expression of connective tissue growth factor (CTGF), collagen, and fibronectin. Notably, TGF-β may also inhibit ECM remodeling by matrix metalloproteinases (MMPs)[23]. Thus, excessive or chronically elevated TGF-β levels can promote scar or keloid formation and fibrosis in adults. Therefore, the new grafts can induce the transformation of M1-type macrophages to M2-type macrophages by promoting the secretion of IL-10 and TGF-β. Additionally, the combination of vascular endothelial growth factor (VEGF) and DAPT not only enhances TGF-β secretion but also restricts its overexpression, which promotes wound healing, reduces fibroplasia, and prevents scar formation.

Matrix metalloproteinases (MMPs) also play crucial roles in cell proliferation, migration (adhesion/dispersion), and differentiation[26]. During the inflammatory response phase of wound healing, collagen peptides generated from MMPs-degraded ECM act as chemokines, promoting the migration of inflammatory cells to the peritrauma site to accelerate wound debridement. Inflammatory cells must degrade the ECM barrier through MMPs in order to reach the periwound area[27]. In addition, the migration of fibroblasts, vascular endothelial cells, squamous epithelial cells, and basal keratinocytes, all of which are crucial for wound healing, also requires the involvement of MMPs[27]. MMPs can stimulate vascular regeneration and accelerate wound healing by regulating growth factors and their receptors within the ECM microenvironment. MMP-1's degradation of type I collagen in the extracellular matrix not only promotes the migration of wound-healing-associated cells but also increases the ratio of type III to type I collagen in the wound, influencing tissue remodeling and accelerating wound healing. Furthermore, MMP-3 can activate and mobilize VEGF and TGF-β in the ECM, enhancing vascular permeability and promoting neoangiogenesis in the granulation tissue[28]. MMP-3 activates and mobilizes VEGF and TGF-β within the ECM to enhance vascular permeability, promote neoangiogenesis in the granulation tissue, and maintain the stability of the endothelial environment, thereby accelerating wound healing[27]. MMP-3 also plays a key role in wound contraction[26]. The new grafts can promote the secretion of MMP-1 and MMP-3, thereby accelerating wound healing.

The present study also has some limitations. Firstly, the physical properties of the grafts were not thoroughly studied or analyzed in this study, which limits the ability to accurately characterize their properties. Secondly, no animal experiments were conducted to evaluate the practical effects of the new grafts. Future studies should focus on detailed physical characterization of the grafts to fully

 doi:10.20944/preprints202509.0226.v1

understand their physical properties. Additionally, animal studies are needed to further assess the application potential of the new grafts at the tissue level.

In summary, the new grafts in this study can enhance monocyte activity, promote the secretion of TNF-α, IL-10, TGF-β, MMP-1, and MMP-3, while limiting the overexpression of TGF-β. These grafts can also induce the transition from M1-type macrophages to anti-inflammatory M2-type macrophages, promote vascular remodeling of peri-wound tissues, improve the inflammatory environment, and accelerate wound healing. Furthermore, they can reduce fibroplasia and prevent scar formation.

Funding: This study was funded by a Fund program: Sichuan Science and Technology Program, No. 2023YFG0227.

Data Availability Statement: All data generated or analysed during this study are included in this article. Further enquiries can be directed to the corresponding author.

Ethics Approval and Consent to Participate: Not applicable.

Conflicts of Interest: The authors have no conflicts of interest to declare.

References

1. Joshi CJ: Hassan A: Carabano M, Galiano RD. Up-to-date role of the dehydrated human amnion/chorion membrane (AMNIOFIX) for wound healing. Expert Opin Biol Ther. 2020;20(10):1125-1131. https://doi.org/10.1080/14712598.2020.1787979 PMID: 32580594.
2. Chen Y, Lyu L, Xue S. Evaluation of human acellular amniotic membrane for promoting anterior auricle reconstruction. Exp Dermatol. 2022;31(5):823-824. https://doi.org/10.1111/exd.14508 PMID: 34847249.
3. Xue SL, Liu K, Parolini O, Wang Y, Deng L, Huang YC. Human acellular amniotic membrane implantation for lower third nasal reconstruction: a promising therapy to promote wound healing. Burns Trauma. 2018;6:34. https://doi.org/10.1186/s41038-018-0136-x PMID: 30574512.
4. Moreira HR, Marques AP. Vascularization in skin wound healing: where do we stand and where do we go? Curr Opin Biotechnol. 2022;73:253-262. https://doi.org/10.1016/j.copbio.2021.08.019 PMID: 34555561.
5. Baron JM, Glatz M, Proksch E. Optimal Support of Wound Healing: New Insights. Dermatology. 2020;236(6):593-600. https://doi.org/10.1159/000505291 PMID: 31955162.
6. Silva LP, Pirraco RP, Santos TC, Novoa-Carballal R, Cerqueira MT, Reis RL, et al. Neovascularization Induced by the Hyaluronic Acid-Based Spongy-Like Hydrogels Degradation Products. ACS Appl Mater Interfaces. 2016;8(49):33464-33474. https://doi.org/10.1021/acsami.6b11684 PMID: 27960396.
7. Distler A, Lang V, Del VT, Huang J, Zhang Y, Beyer C, et al. Combined inhibition of morphogen pathways demonstrates additive antifibrotic effects and improved tolerability. Ann Rheum Dis. 2014;73(6):1264-8. https://doi.org/10.1136/annrheumdis-2013-204221 PMID: 24445254.
8. Kloc M, Ghobrial RM, Wosik J, Lewicka A, Lewicki S, Kubiak JZ. Macrophage functions in wound healing. J Tissue Eng Regen Med. 2019;13(1):99-109. https://doi.org/10.1002/term.2772 PMID: 30445662.
9. Bygd HC, Forsmark KD, Bratlie KM. Altering in vivo macrophage responses with modified polymer properties. Biomaterials. 2015;56:187-97. https://doi.org/10.1016/j.biomaterials.2015.03.042 PMID: 25934291.
10. Kumar M, Coburn J, Kaplan DL, Mandal BB. Immuno-Informed 3D Silk Biomaterials for Tailoring Biological Responses. ACS Appl Mater Interfaces. 2016;8(43):29310-29322. https://doi.org/10.1021/acsami.6b09937 PMID: 27726371.
11. Kumar M, Nandi SK, Kaplan DL, Mandal BB. Localized Immunomodulatory Silk Macrocapsules for Islet-like Spheroid Formation and Sustained Insulin Production. ACS Biomater Sci Eng. 2017;3(10):2443-2456. https://doi.org/10.1021/acsbiomaterials.7b00218 PMID: 33445302.
12. Sharifiaghdam M, Shaabani E, Faridi-Majidi R, De Smedt SC, Braeckmans K, Fraire JC. Macrophages as a therapeutic target to promote diabetic wound healing. Mol Ther. 2022;30(9):2891-2908. https://doi.org/10.1016/j.ymthe.2022.07.016 PMID: 35918892.

 doi:10.20944/preprints202509.0226.v1

13. Lucas T, Waisman A, Ranjan R, Roes J, Krieg T, Muller W, et al. Differential roles of macrophages in diverse phases of skin repair. J Immunol. 2010;184(7):3964-77. https://doi.org/10.4049/jimmunol.0903356 PMID: 20176743.
14. Aitcheson SM, Frentiu FD, Hurn SE, Edwards K, Murray RZ. Skin Wound Healing: Normal Macrophage Function and Macrophage Dysfunction in Diabetic Wounds. Molecules. 2021;26(16) https://doi.org/10.3390/molecules26164917 PMID: 34443506.
15. Jin GR, Hwang SB, Park HJ, Lee BH, Boisvert WA. Microinjury-Induced Tumor Necrosis Factor-alpha Surge Stimulates Hair Regeneration in Mice. Skin Pharmacol Physiol. 2023;36(1):27-37. https://doi.org/10.1159/000528403 PMID: 36693328.
16. Naserian S, Abdelgawad ME, Afshar BM, Ha G, Arouche N, Cohen JL, et al. The TNF/TNFR2 signaling pathway is a key regulatory factor in endothelial progenitor cell immunosuppressive effect. Cell Commun Signal. 2020;18(1):94. https://doi.org/10.1186/s12964-020-00564-3 PMID: 32546175.
17. Wong MM, Chen Y, Margariti A, Winkler B, Campagnolo P, Potter C, et al. Macrophages control vascular stem/progenitor cell plasticity through tumor necrosis factor-alpha-mediated nuclear factor-kappaB activation. Arterioscler Thromb Vasc Biol. 2014;34(3):635-43. https://doi.org/10.1161/ATVBAHA.113.302568 PMID: 24458710.
18. Huang Y, Li S. Detection of characteristic sub pathway network for angiogenesis based on the comprehensive pathway network. BMC Bioinformatics. 2010;11 Suppl 1(Suppl 1):S32. https://doi.org/10.1186/1471-2105-11-S1-S32 PMID: 20122205.
19. Shams F, Moravvej H, Hosseinzadeh S, Mostafavi E, Bayat H, Kazemi B, et al. Overexpression of VEGF in dermal fibroblast cells accelerates the angiogenesis and wound healing function: in vitro and in vivo studies. Sci Rep. 2022;12(1):18529. https://doi.org/10.1038/s41598-022-23304-8 PMID: 36323953.
20. Souza LV, De Meneck F, Oliveira V, Higa EM, Akamine EH, Franco M. Detrimental Impact of Low Birth Weight on Circulating Number and Functional Capacity of Endothelial Progenitor Cells in Healthy Children: Role of Angiogenic Factors. J Pediatr. 2019;206:72-77.e1. https://doi.org/10.1016/j.jpeds.2018.10.040 PMID: 30798839.
21. Mills CD. Anatomy of a discovery: m1 and m2 macrophages. Front Immunol. 2015;6:212. https://doi.org/10.3389/fimmu.2015.00212 PMID: 25999950.
22. Mantovani A, Biswas SK, Galdiero MR, Sica A, Locati M. Macrophage plasticity and polarization in tissue repair and remodelling. J Pathol. 2013;229(2):176-85. https://doi.org/10.1002/path.4133 PMID: 23096265.
23. Ehnert S, Rinderknecht H, Liu C, Voss M, Konrad FM, Eisler W, et al. Increased Levels of BAMBI Inhibit Canonical TGF-beta Signaling in Chronic Wound Tissues. Cells. 2023;12(16) https://doi.org/10.3390/cells12162095 PMID: 37626905.
24. Ruiz-Canada C, Bernabe-Garcia A, Liarte S, Rodriguez-Valiente M, Nicolas FJ. Chronic Wound Healing by Amniotic Membrane: TGF-beta and EGF Signaling Modulation in Re-epithelialization. Front Bioeng Biotechnol. 2021;9:689328. https://doi.org/10.3389/fbioe.2021.689328 PMID: 34295882.
25. Penn JW, Grobbelaar AO, Rolfe KJ. The role of the TGF-beta family in wound healing, burns and scarring: a review. Int J Burns Trauma. 2012;2(1):18-28. PMID: 22928164.
26. Huth S, Huth L, Marquardt Y, Cheremkhina M, Heise R, Baron JM. MMP-3 plays a major role in calcium pantothenate-promoted wound healing after fractional ablative laser treatment. Lasers Med Sci. 2022;37(2):887-894. https://doi.org/10.1007/s10103-021-03328-8 PMID: 33990899.
27. Krishnaswamy VR, Mintz D, Sagi I. Matrix metalloproteinases: The sculptors of chronic cutaneous wounds. Biochim Biophys Acta Mol Cell Res. 2017;1864(11 Pt B):2220-2227. https://doi.org/10.1016/j.bbamcr.2017.08.003 PMID: 28797647.
28. Mu X, Bellayr I, Pan H, Choi Y, Li Y. Regeneration of soft tissues is promoted by MMP1 treatment after digit amputation in mice. PLoS One. 2013;8(3):e59105. https://doi.org/10.1371/journal.pone.0059105 PMID: 23527099.

 doi:10.20944/preprints202509.0226.v1

disclaim responsibility for any injury to people or property resulting from any ideas, methods, instructions or products referred to in the content.